ISSN (Print) 1226-1750
ISSN (Online) 2233-6656
Journal of Magnetics 21(1), 125-132 (2016) http://dx.doi.org/10.4283/JMAG.2016.21.1.125

Buffer-Optimized High Gradient Magnetic Separation: Target Cell Capture Efficiency is Predicted by Linear Bead-Capture Theory

Shahid Waseem[1,2], Rachanee Udomsangpetch[1], and Sebastian C. Bhakdi[1,3]*

[1]*Department of Pathobiology, Faculty of Science, Mahidol University, Rama 6 Road, Bangkok 10400, Thailand*
[2]*Department of Biochemistry, Faculty of Biological Sciences, Quaid-i-Azam University, Islamabad 45320, Pakistan*
[3]*X-Zell Biotec Co., Ltd., Na-Nakorn Building, 99/349, Moo 2, Chaengwattana Road, Laksi, Bangkok 10210, Thailand*

(Received 1 October 2015, Received in final form 21 December 2015, Accepted 22 December 2015)

High gradient magnetic separation (HGMS) is the most commonly used magnetic cell separation technique in biomedical science. However, parameters determining target cell capture efficiencies in HGMS are still not well understood. This limitation leads to loss of information and resources. The present study develops a bead-capture theory to predict capture efficiencies in HGMS. The theory is tested with CD3- and CD14-positive cells in combination with paramagnetic beads of different sizes and a generic immunomagnetic separation system. Data depict a linear relationship between normalized capture efficiency and the bead concentration. In addition, it is shown that key biological functions of target cells are not affected for all bead sizes and concentrations used. In summary, linear bead-capture theory predicts capture efficiency (E_t) in a highly significant manner.

Keywords : high gradient magnetic separation, capture efficiency, recovery rate, CD3-positive cells, CD14-positive cells

1. Introduction

Over the past three decades, magnetic cell separation has been established as an important tool in biomedical research. To isolate a particular subgroup of cells from a heterogeneous cell suspension, target cells are labelled with paramagnetic beads that are attached to specific antibodies. Commercially available techniques include conventional magnetic separation (Dynal, Invitrogen, Carlsbad, USA), the technically more sophisticated quadrupole separation (EasySep, Stem Cell techniques, Vancouver), and high gradient magnetic separation (MACS, Miltenyi Biotec, Germany). Bead sizes range from several micrometres down to tens of nanometres, and the choice of bead size plays an important role as to which magnetic separation technique can be employed. Micrometre-sized beads can be separated by conventional magnets but usually require removal after separation since they interfere with flow cytometric or light microscopic readout systems. It has also been reported that these larger bead sizes can lead to polyvalent binding, or in other words, cross linking of receptors which leads to activation of sensitive cells and/or to endocytosis of beads [1]. Currently, nanosized beads are therefore preferred for most applications. However, because of the significantly lower amounts of paramagnetic material attached to each cell, they require one of the two more sophisticated magnetic separation techniques.

The most widespread technique for separation of very weakly paramagnetic bodies is high gradient magnetic separation (HGMS). In HGMS, a matrix of thin filaments or spheres of ferromagnetic material is placed in a strong homogeneous magnetic field. With this technique, magnetic field gradients of up to 100 T/cm can be created at the surface of the matrix [2]. Early work on generic HGMS systems [3, 4] eventually led to the development of the MACS HGMS system [5]. Today, the MACS system is still the only viable commercially available HGMS technique in cell biology, with over 12000 studies published during the past two decades [6]. The MACS system relies on HGMS in combination with 20–100 nm diameter paramagnetic beads. However, while separation purities are generally reported to be acceptable, capture efficiencies (E_t = [target cells isolated]/[total target cells

©The Korean Magnetics Society. All rights reserved.
*Corresponding author: Tel: +66-80-599-7961
Fax: +66-25-761-437, e-mail: sbhakdi@gmail.com

loaded]) are not always consistent between different researchers and different target cell types. In many cases this leads to loss of information and resources [7].

The present study develops linear bead-capture theory to describe practical predictive parameters for E_t in HGMS. The theory is tested by labelling two different cell types with commercially available magnetic beads of 50 nm and 100 nm diameter. Buffer-optimized HGMS serves as a readout system for E_t, as described previously [8], and functional assays demonstrate viability of isolated cells.

2. Theory

2.1. Capture of beads by cells

We treat the cells and beads as spheres. The mean speed of a body in equilibrium with its surroundings is inversely proportional to the square root of its mass. The smallest cell (7 μm diameter) has a mass 70^3 times that of the largest bead used (0.1 μm diameter), assuming both have the same density. Hence the unattached beads have an average speed which is at least $\sqrt{70^3} \sim 600$ times that of the cells. We therefore regard the cells as being stationary and subject to a flux of beads κn where n is the number density of the unattached viable beads and κ is a constant [9]. Let $B(t)$ and $W(t)$ denote, respectively, the total numbers of beads attached to antigens on the target cells and bound non-specifically (either to target cells or to other cells) at time t. The beads are added at $t = 0$ and so $B(0) = W(0) = 0$. The number of unattached viable beads, $N(t) = N(0)-B(t)-W(t)$, and $n = N/V$ where V is the volume of the suspension. Let A_{sb} be the maximum possible total cell surface area taken up by specifically bound beads. If r_b is the radius of a bead then $A_{sb} = \alpha_t N_c b_{max}\ \pi r_b^2$ where N_c is the number of cells, α_t is the fraction of cells which are target cells, and b_{max} is the maximum number of beads that can be bound to antigens on a target cell and is given by

$$b_{max} = \min(a,\ \varphi d_t^2/r_b^2)$$

where a is the number of antigens per target cell and ϕ is the fraction of the cell surface area that can be covered by beads. We assume that $\phi = \pi/12 = 0.9069$, the value for close packing of discs on a plane. The total surface area available for non-specific binding before any beads are present on all the cells is given by

$$A_{nsb} = \pi\varphi N_c \sum_t a_t d_t^2 - A_{sb}$$

where d_i and α_i are the root mean squared diameter of and proportion of cells that are cell type i.

To avoid making the model too detailed, we make the following assumptions: (i) the antigens are uniformly distributed on the target cells (ii) beads only attach to areas not already occupied by a bead (iii) a bead has a chance of attaching to an antigen if the point at which the bead initially touches the cell is less than r_b from the antigen (iv) non-specific binding never approaches saturation (i.e., $W\pi r_b^2 << A_{nsb}$).

Then we have

$$\frac{dB}{dt} = \beta kn(A_{sb} - B\pi r_b^2), \tag{1}$$

$$\frac{dW}{dt} = \gamma kn(A_{nsb} - W\pi r_b^2) \tag{2}$$

where β and γ are the fraction of times that a viable bead sticks when colliding with, respectively, an antigen or another part of the cell surface. Dividing (1) and (2) by $\alpha_t N_c$ and N_c, respectively, gives

$$\frac{db}{dt} = \beta\pi r_b^2\kappa(n_0 - a_t n_c b - n_c w)(b_{max} - b) \tag{3}$$

$$\frac{dw}{dt} = \gamma\pi r_b^2\kappa(n_0 - a_t n_c b - n_c w)(w_{max} - w) \tag{4}$$

where b is the mean number of beads attached to antigens on a target cell, w is the mean number of non-specifically bound beads on any cell, n_0 is the initial number density of viable unattached beads, and

$$w_{max} = \frac{\varphi}{r_b^2}\sum_t a_t d_t^2 - a_t b_{max}$$

The coupled nonlinear equations (3) and (4) cannot be solved analytically. However, the behaviour of b and w is straightforward; both increase monotonically from zero and will saturate as either factor in brackets on the right-hand sides approaches zero. When $b << b_{max}$, $w << w_{max}$ and $a_t n_c b + n_c w << n_0$ the right-hand sides are approximately constant and are both proportional to n_0. We refer to this case as the linear regime.

The number of beads attached to target cells is $B + (A_{nsbt}/A_{nsb})W$ where the total area not occupied by antigens on the target cells, $A_{nsbt} = \pi\alpha_t N_c \varphi d_t^2 - A_{sb}$. Hence c_t, the mean number of beads attached to a target cell, is given by

$$c_t = b + \left(\varphi d_t^2 - \frac{b_{max} r_b^2}{w_{max} r_b^2}\right) w \tag{5}$$

In the linear regime c_t is therefore also proportional to n_0.

2.2. HGMS capture efficiency

According to [10], the capture efficiency for a cell of type i (i.e., [the number of cells of type i captured]/[the number of cells of type i that enter column]) is given by

$$E_t = 1 - \exp\left(-\frac{(h)d_t^2 FL\chi_i MB_0}{36\pi\eta r_p^2 b_p v f}\right) \quad (6)$$

where (h) is the geometric factor (which is 4/3 for a random filter), F is the filter filling factor (0.12 in our case), L is the filter length (5 cm), M is the saturation magnetization of the matrix material (1.2 MA/m). B_0 is the applied magnetic flux density (0.7 T), η is the fluid dynamic viscosity (2×10^{-3} kgm^{-1} s^{-1}), r_{pbp} is the radius of the particle buildup profile (which is initially equal to the radius of the wires, 30 μm), and v_{f} is the mean fluid speed (2.0 mm/s). χ_i is the volume magnetic susceptibility of a cell of type i including the attached beads minus that of the fluid and is given approximately by

$$\chi_i = \left(\frac{2r_b}{d_i}\right)^3 fc_i\chi_{Fe} \quad (7)$$

where f is the volume fraction of a bead occupied by the magnetite (0.18), χ_{Fe} is the volume magnetic susceptibility of the magnetite (0.61), and c_i is the number of beads per cell of type i. Using (6) and (7) with $E_{\mathrm{t}} = 0.95$ gives

$$c_t = \frac{9\pi\log(20)\eta r_{pbp}^2 v_f d_t}{2(h)FLMB_0 r_b^3 f\chi_{Fe}} \quad (8)$$

which in our case, with $d_{\mathrm{t}} = 10$ μm and 50 nm beads, evaluates to 130 which is much less than $b_{\max}$. Thus we can safely assume that the linear regime applies and so c_{t} is proportional to n_0. We may therefore write

$$Q \equiv -\log(1 - E_{\mathrm{t}}) \propto n_0. \quad (9)$$

The constant of proportionality depends on the bead capture probabilities β and γ which will differ among blood donors. We remove the effect of having a variety of blood donors by dividing Q by the constant of proportionality (calculated from the data obtained using cells of each donor using a regression line through the origin) to obtain the normalized quantity q which we therefore expect to obey $q = n_0$.

3. Materials and Methods

3.1. Mononuclear cell preparation

Human peripheral blood was obtained from voluntary donors after informed consent and peripheral blood mononuclear cells were separated by density centrifugation by equal ratio (1:1) of blood to Lymphoprep (Axis-Shield PoC AS, Oslo) at 2000g for 20 min. Mononuclear cells (MNCs) at the interface were collected and re-suspended in HGMS buffer (X-Zell Biotech Co. Ltd., Bangkok). MNC were counted using a haemocytometer (Boeco, Germany). Blood sampling (ID 04-52-39) was approved through Ethical Committee of Research on Human being, Ramathebodi Hospital, Faculty of Medicine, Mahidol University, Bangkok, Thailand.

3.2. Isolation of CD3- and CD14-positive cells

A customized HGMS magnet, HGMS columns, HGMS buffers, and HGMS beads were from X-Zell Biotech Co. Ltd., Bangkok. The HGMS magnet provided a minimum magnetic field strength of 0.7 T between the poles, as determined by a DC-Gaussmeter (alpha-Lab Inc., Salt Lake City, Utah). Positive isolation of cells was performed according to the manufacturer's protocol. Briefly, MNCs were incubated with 100 μl of human AB serum (Gemini Bio Products Inc., California) for blocking of Fc receptors. Varying volumes of 50 nm or 100 nm anti-CD3 or anti-CD14 HGMS beads were added and the MNCs were incubated in HGMS buffer for 30 min at 4 ºC. Cells were gently shaken every 10 min. The bead concentration was adjusted to between 1.5 and 13 × 10^{12} beads/ml. The target cell concentration was between 0.75 and 20 × 10^6 cells/ml. After incubation, cells were washed once with PBS (Biochrom AG, Berlin), pelleted at 400 g for 10 min and resuspended in HGMS buffer. HGMS columns were filled with HGMS buffer in an upright position to evacuate air by upward displacement. After removing the remaining air bubbles by gentle finger tapping, a 20G/1-inch injection needle was connected to the stopcock. The column was placed between the poles of the HGMS magnet and equilibrated for 5 min. The stopcock of the HGMS column was opened, 10^7 MNCs were applied for each experiment and the column was rinsed with 30 ml of HGMS buffer. After this, the stopcock was closed and the column was removed from the magnet. The column was flushed retrogradely with 12 ml of PBS. The eluate containing the target cells was collected, washed once by centrifugation at 1,100 g for 10 min, Giemsa stained, and analysed by light microscopy.

3.3. Phagocytic assay

To test the phagocytic activity of isolated CD14-positive cells, phagocytic assays were adapted from [11]. Briefly, 1 × 10^5 isolated CD14-positive cells were suspended in culture media (RPMI 1640 + 10% FBS) (both from Biochrom, Berlin) and incubated with 1 × 10^8 0.45 μm-diameter latex beads in 24-well cell culture plates (Becton Dickinson, USA) at 37 ºC and 5% CO_2. Phago-

cytic activity was analysed after 1.5 h. Cells were washed with 2% sucrose/PBS solution (USB Corporation, Cleveland/Biochrom, Berlin) to remove non-ingested latex beads (kindly synthesized for us by Prof. Pramuan Tungboriboonrat, Mahidol University). The entire protocol was performed under sterile conditions. After incubation, bead-containing and bead-free macrophages (MØ) were counted (per 1000 cells) under a phase contrast microscope (Olympus Optical Co., Tokyo) and their ratio calculated. After counting, isolated cells were subjected to cytospin, fixed and stained with Giemsa, and observed (at 400 × magnification) under a light microscope (Olympus Optical Co., Tokyo).

3.4. Parasite culture

Plasmodium falciparum strain AMB47 was cultivated in O-positive whole blood as described in [12]. Peripheral blood was obtained from voluntary donors and human serum from the blood bank of Ramathibodi Hospital, Bangkok. Blood was stored at 4 ºC for at least one week to reduce viable leukocytes before parasite culture. Infected red blood cells (iRBCs) were cultured in malaria culture media (MCM) (10.43 g RPMI 1640 powder medium, 7.5% sodium bicarbonate (both Biochrom AG, Berlin), 40 μg/ml gentamycin (Gibco), 25 mM 4-(2-hydroxyethyl)-1-piperazine ethane-4-sulphonic acid (HEPES) and 200 mM hypoxanthine (both from Sigma, Hamburg) supplemented with 10% non-inactivated human serum) in 75 cm^2 cell culture flasks (Corning Inc., New York) at 37 ºC with 5% CO_2. The parasite culture medium was changed every 24 h. The culture was maintained in 5% haematocrit.

3.4.1. Synchronization of parasites

Parasites were synchronized to ring stages by treating with 5% sorbitol (Merck, Germany) following [13]. The parasite culture was washed twice (1000 *g*, 90 s) with MCM after synchronization. Synchronized parasites in 5% haematocrit were then resuspended in MCM. Synchronization was evaluated by Giemsa staining.

3.4.2. Cryopreservation

For stock, 0.33 volumes of glycerolyte (Sigma, Hamburg) were added dropwise to packed iRBCs, mixed gently, and incubated at room temperature for 5 min. After incubation, 1.33 volumes of glycerolyte were added, frozen in cryovials (Corning Inc., New York) at −80 ºC overnight, and then stored in liquid nitrogen.

3.4.3. Thawing

Cryovials were thawed at 37 ºC and parasitized blood was transferred to 50 ml centrifuge tubes (Corning Inc., New York). 0.2 volumes of cold 12% NaCl (Merck, Darmstadt) solution were mixed gently with thawed iRBCs and incubated for 5 min at room temperature. Next, 10 volumes of cold 1.6% NaCl solution were added gently and centrifuged at 300 *g* for 10 min at 4 ºC. After removal of the supernatant, 10 volumes of cold 0.9% NaCl were added and mixed gently and centrifuged as above. The pellets were resuspended in MCM, and parasitemia and viability were measured by Giemsa staining.

3.5. Proliferation assay

Functional capacity of isolated CD3-positive cells was tested by proliferation and viability assays. The protocol was adopted from [14] with modifications. Briefly, MNCs were separated by Lymphoprep and cultured in a 75 cm^2 cell culture flask in 35 ml RPMI 1640 with 10% FBS at 37 ºC in 5% CO_2 for 1.5 h. After incubation, supernatant containing suspended lymphocytes was removed. Monocytes attached to the flask surface were washed gently with 10 ml RPMI 1640 + 10% FBS. Finally, 5 ml of the same media was added to cover the monolayer of attached monocytes and incubated at 4 ºC overnight. On day 2, monocytes were removed from the pre-incubated cell culture flask by cell scraper (SPL Lifescience, Korea).

HGMS isolation of CD3-positive cells was performed from MNCs obtained from peripheral blood of the same donor. Isolated monocytes and CD3-positive cells were counted by haemocytometer. Three experimental conditions were set per experiment. For all conditions, the initial cell count was 2×10^5 cells/well for MØ and 1×10^6 cells/well for CD3-positive cells. Cells were incubated in a 24-well cell culture plate (Becton Dickinson, USA) in 1 ml of media. Condition 1 comprised only MØ and unstimulated CD3-positive cells.

In condition 2, *P. falciparum* iRBCs were used for stimulation of CD3-positive cells, as described in [15]. MØ were incubated with iRBCs for 4 h at 37 ºC and 5% CO_2 before adding CD3-positive cells. Cell concentrations were set at 1:5:5 for MØ:CD3-positive cells:iRBCs, respectively. Condition 3 was identical to condition 1 except that CD3-positive cells were stimulated with 2 μg/ml leucoagglutinin (PHA-L) (Biochrom, Cambridge, UK). Proliferation and viability of CD3-positive cells was assayed at four different times (day 2, day 4, day 6, and day 8). Analysis was performed by Giemsa staining and light microscope. The entire protocol was performed under sterile conditions.

3.6. Mitotic assay

After counting CD3-positive cells, the remaining cells

were incubated with 3 μg/ml cytochalasin B (Sigma-Aldrich, Germany) for 18–20 h at 37 ºC and 5% CO_2 as described in [16]. After incubation, cells were harvested, subjected to cytospin, fixed for 10 min, and stained with Giemsa. Bi-, tri- and tetra-nucleated CD3-positive cells were analysed under light microscope. The mitotic index (MI), given by

$$MI = \sum_{r=1}^{4} r\,\eta_r \div \sum_{r=1}^{4} \eta_r$$

where η_r is the number of cells which are r-nucleated, was calculated from 1000 cells.

4. Results

4.1. Testing of predictive power of linear bead-capture theory

Predictive accuracy of linear bead-capture theory was examined with two different bead sizes and two different cell types, as described in the materials and methods. For both bead sizes, purities of CD3- and CD14-positive cells after magnetic separation were at least 95% in all experiments.

If values of $\log(1 - E_t)$ are plotted against bead concentration n_0 then the theory predicts that the points should lie on a straight line through the origin. Experimental results were normalized as described in section 2.2. Data of q, the normalized value of $-\log(1 - E_t)$, was combined from a total of 15 different blood donors and plotted against n_0 as shown in Fig. 1. R^2 values range from 0.77–0.98.

For 50 nm beads, an E_t of over 80% was consistently achieved for bead concentrations > 8.6×10^{12} ml^{-1} and target cell concentrations > 4.0×10^6 ml^{-1} for CD14-positive cells, and for > 6.0×10^{12} beads/ml and > 10.4×10^6 target cells/ml for CD3-positive cells. For 100 nm beads, such capture efficiencies were obtained with > 0.72×10^{12} beads/ml and > 3.0×10^6 target cells/ml for CD14-positive cells, and > 0.32×10^{12} beads/ml and > 1.7×10^6 target cells/ml for CD3-positive cells (data not shown).

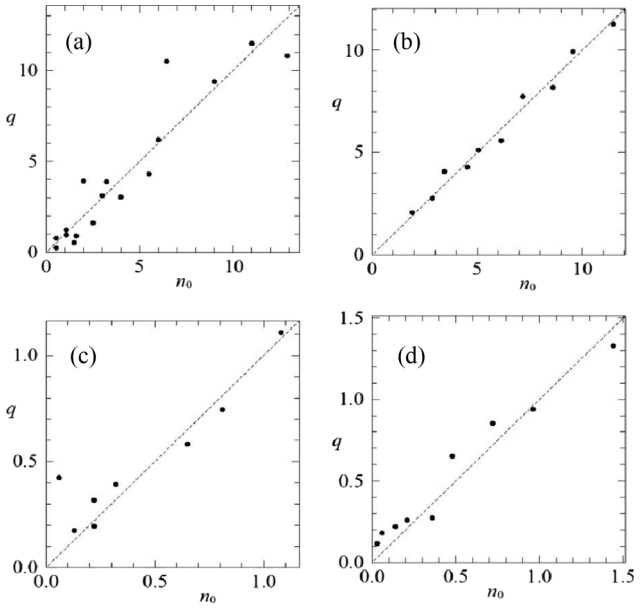

Fig. 1. Normalized $-\log(1 - E_t)$ against bead concentration n_0 (both in units of 10^{12} ml^{-1}) for both target cell types and bead diameters: (a) CD3 50 nm ($R^2 = 0.88$) (b) CD14 50 nm ($R^2 = 0.98$) (c) CD3 100 nm ($R^2 = 0.77$) (d) CD14 100 nm ($R^2 = 0.93$).

Morphological examination of isolated target cells (CD3- and CD14-positive cells) showed no discernible difference in their morphologies (Fig. 2a-d).

4.2. Functional assays

4.2.1. CD3-positive cells proliferation and mitotic assay

To demonstrate the viability of CD3-positive cells after HGMS, cells were subjected to proliferation assays. Figure 3a depicts the proliferation pattern of isolated CD3-positive cells. Experiments were continued over 8 days, with three different conditions as described in the materials and methods. Condition 1 (MØ and CD3-

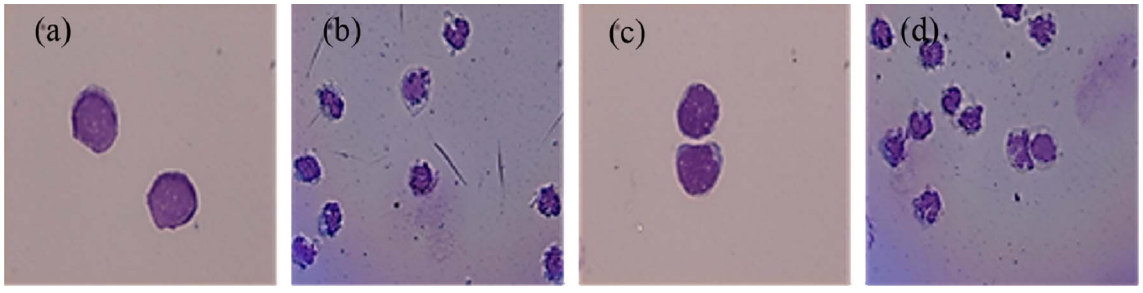

Fig. 2. (Color online) Morphologies of captured target cells. (a) CD3 50 nm (b) CD14 50 nm (c) CD3 100 nm (d) CD14 100 nm. Images in this and subsequent figures were taken at 400 × magnification for CD3-positive cells and 200 × magnification for CD14-positive cells by light microscope.

positive cells without stimulation) served as control and did not show significant proliferation at any time. In condition 2 (MØ + iRBCs + CD3-positive cells), proliferation of CD3-positive cells was seen from day 2 until day 6. The number of cells increased 1.5-, 2.4- and 2.8-fold on days 2, 4, and 6, respectively. A decrease in the number of cells was observed on day 8. With condition 3 (CD3-positive cells co-cultured with MØ stimulated with PHA-L), the number of cells increased 1.6-, 2.8- and 3.5-fold on days 2, 4, and 6, 215 respectively. CD3-positive cell numbers decreased after day 6 (Fig. 3a).

MI of isolated CD3-positive cells is shown in Fig. 3b. MI for both conditions 2 and 3 was higher than controls. However, only MI for condition 3 was significantly higher than the control ($p < 0.05$). On day 6, over 80% of PHA-stimulated CD3-positive cells and 30% of iRBC-stimulated CD3-positive cells were binucleated as compared to 3% binucleated cells in the control. MI at day 2, day 4, day 6 and day 8 was respectively, 0.97, 1.09, 1.41, and 0.89 for unstimulated CD3-positive cells, 0.98, 1.22, 1.74, and 1.13 for iRBC-stimulated CD3-positive cells, and 1.3, 1.54, 2.5, and 1.19 for PHA-stimulated CD3-positive cells. Unstimulated CD3-positive cells showed hardly any proliferation and retained their cellular morphology and membrane integrity (Fig. 3c). However, iRBC-stimulated (yellow arrow head) and PHA-stimulated (black arrow heads) CD3-positive cells showed clear binuclei on day 6. Cells with tri- or tetra-nuclei were also observed (pictures not shown). Fewer proliferating CD3-positive cells were found on day 2 and day 4 (pictures not shown).

4.2.2. Phagocytic assay

To test key functions of CD14-positive cells after HGMS, phagocytic assays were performed by latex bead

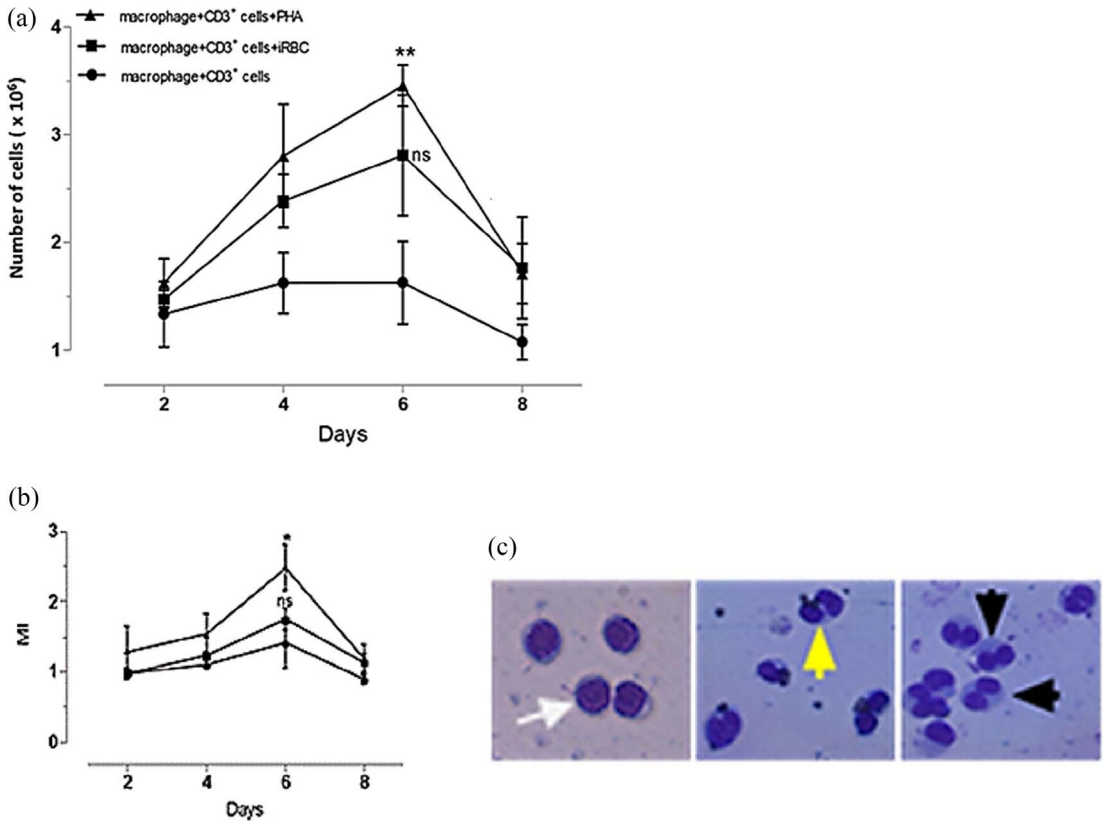

Fig. 3. (Color online)Functional analysis of CD3-positive cells isolated by HGMS with 50 nm magnetic beads by proliferation and mitotic assays. (a) The MØ:CD3-positive cell:iRBC ratio was set at 1:5:5 (iRBCs only in condition 2). Significant proliferation of CD3-positive cells was observed in conditions 2 and 3 ($p < 0.01$). (b) For mitotic assays, the number of binucleated cells was counted. Mitotic index (MI) for stimulated (with iRBCs and PHA-L) and unstimulated CD3-positive cells is shown. MI of CD3-positive cells stimulated with PHA-L was significantly higher than controls on day 6 ($p < 0.05$) compared to unstimulated CD3-positive cells on day 6. (c) Representative morphology of binucleated CD3-positive cells is shown here (Giemsa stained slides of day 6 for all three experimental conditions). White arrow shows unstimulated CD3-positive cells, yellow arrow shows binucleated cells in iRBC stimulated CD3-positive cells, and black arrows show binucleated CD3-positive cells in PHA-stimulated condition. Data are collected from three independent experiments and calculated as mean ± SE. ns = not significant.

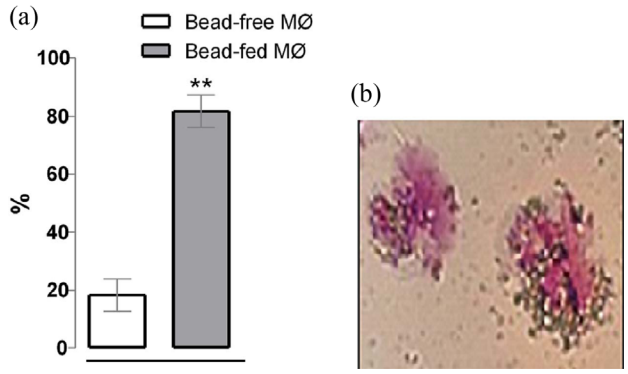

Fig. 4. (Color online) Phagocytic assay. Ingestion of latex beads (0.45 μm) by CD14-positive cells-derived macrophages (MØ), after isolation by HGMS system with 50 nm magnetic beads. (a) Percentages of bead-free (white bar) and bead-fed (grey bar) MØ were calculated from a total count of 1000 cells. MØ (1×10^5) were exposed to latex beads (1×10^8) for 1.5 h in a 24-well cell culture plate and then observed under a phase contrast microscope. (b) MØ were also subjected to cytospin for Giemsa staining to see latex beads inside cells (a representative photograph of bead-fed MØ). Data are calculated from three independent experiments as mean ± SE.

(0.45 μm) ingestion assay. Around 82% of cells showed ingestion of latex beads in 1.5 h as shown in Fig. 4a. Phagocytosis was statistically significant ($p < 0.01$). A representative photograph of cells with ingested latex beads is shown in Fig. 4b. Identical results were observed after HGMS of CD14-positive cells with both 50 nm and 100 nm magnetic beads (100 nm bead data not shown).

5. Discussion

In spite of the three decade-long history of HGMS in biomedical research, very few studies are available that examine the influence of physical parameters on capture efficiency E_t. This seems surprising given that not only the key parameters (drag force and magnetic force) of a conventional HGMS apparatus can be considered constant, but also that the physical parameters of magnetically labelled cells vary only in a very narrow range. More specifically, cell size and receptor density are well characterized for a large number of cell sub-populations, and together with known parameters of the HGMS apparatus, it can be hypothesized that consistent separation results should be achievable. The present study developed linear bead-capture theory which identifies bead concentration as the single most important parameter to predict E_t.

The study chose to focus on CD3-positive cells, which are fairly constant in both size and CD3 receptor expression [17], and CD14-positive cells which exist in two ranges of diameters, both with fairly constant CD14 receptor expression [11, 18, 19]. These two cell types, together with two different bead sizes, served as a model to test linear bead-capture theory on a generic, buffer-optimized HGMS system.

The theory predicts that $\log(1 - E_t)$ is proportional to the number of beads bound to target cells. When the number of beads bound to target cells is small, this number of bound beads is in turn proportional to the initial concentration of beads during incubation of cells with beads. In other words, plots of $\log(1 - E_t)$ against initial bead concentration n_0 for various bead and target cell concentrations are expected to lie on a straight line through the origin.

Results of the present study confirm that the theory predicts E_t in a highly significant manner, with R^2 values ranging from 0.77–0.98 (Fig. 1). As predicted by linear bead-capture theory, it is clear that bead concentration and bead size must be optimized, while taking into account the surface receptor density of target cells, to achieve consistently high E_t.

Interestingly, variation of bead and target cell concentration, or in other words, variation of the bead/cell ratio and E_t had no influence on isolation purity. Positive selection of CD3- and CD14-positive cells by the HGMS system led to over 95% purity in all experiments.

From the above, it should now become possible to better predict E_t for different cell types and bead sizes. For example, CD34-positive haematopoietic stem cells were described to have receptor densities of around 50000 receptors per cell [20] or, in other words, around 2 times lower receptor density than CD3- and CD14-positive cells. At the same time it is known that E_t for CD34-positive cells in conventional HGMS systems are rather inconsistent [21]. It may now be hypothesized that commonly used protocols have not optimized the bead concentration during labelling of cells with beads and/or that commercially available 50 nm beads are not able to confer sufficient magnetic susceptibility to cells with such low receptor densities.

In the latter case, use of 100 nm beads would increase magnetic susceptibility by one order of magnitude and should therefore lead to much more consistent results.

Since linear bead-capture theory might require different bead sizes for optimization of capture efficiency, the present study also examined the effect of varying bead diameters on cellular functions. HGMS-purified CD14- and CD3-positive cells were assessed by phagocytic and proliferation assays. Assays were performed without prior removal of beads, as is sometimes recommended [22].

Viability and proliferation rates of CD3-positive cells remained unchanged after separation with both 50 nm and 100 nm beads. Mitotic indices of CD3-positive cells were highest when stimulated with PHA-L, while stimulation with iRBCs resulted in lower, but still significant, mitosis. The latter does not seem surprising given the entirely different mechanisms of stimulation: PHA-L directly recruits T lymphocytes to undergo mitosis [23] whereas iRBCs are phagocytosed by monocytes and by antigens presented to T lymphocytes [24].

To examine functionality of CD14-positive cells isolated by HGMS, the inert latex beads ingestion model was adopted. Ingestion of latex beads in monocytes was previously explained as a measure of frustrated phagocytosis; over 80% of phagocytically active monocytes reflect optimal cellular engagement with inert latex beads [25, 26]. Results of the present study show that for isolation of CD14-positive cells with both 50 nm and 100 nm beads, over 80% of cells were phagocytically active. Also, it was observed that adhesion capacities of CD14-positive cells on cell culture dishes were over 80% (data not shown).

In summary, linear bead-capture theory predicts E_t in a highly significant manner. Moreover, E_t is independent of the source and the type of target cells but dependent on the bead concentration. Biological functions of the target cells remain intact after HGMS. However, assay-dependent optimization of bead concentration and bead size seems feasible.

Further studies corroborating linear bead-capture theory are certainly warranted. For example, the theory contains various parameters whose values are difficult to obtain theoretically. The most important of these are the quantities $\beta\kappa$ and $\gamma\kappa$ which relate to the rate at which beads bind to the cells (see section 2.1). To further refine the predictive power of the theory by finding these values more directly, data on the number of beads attached as a function of time will be needed.

Acknowledgements and Declarations

We thank Prof. Pramuan Tungboriboonrat, Chemistry Department, Mahidol University for synthesizing the latex beads. This study was supported by a Thailand Research Fund grant (BRG5380006). The funding source had no involvement in the design of this study, collection, analysis and interpretation of the data, in writing the manuscript and in the decision to submit the paper to this journal. SCB is the director of a company developing HGMS systems for biomedical research. The other authors declare that they have no competing interests.

References

[1] A. Øren, C. Husebø, A.-C. Iversen, and R. Austgulen, J. Immunol. Meth. **303**, 1 (2005).
[2] J. Oberteuffer, IEEE Trans. Magn. **9**, 303 (1973).
[3] F. Paul, S. Roath, and D. Melville, Br. J. Haematol. **38**, 273 (1978).
[4] F. Paul, S. Roath, D. Melville, D. Warhurst, and J. Osisanya, The Lancet **318**, 70 (1981).
[5] S. Miltenyi, W. Müller, W. Weichel, and A. Radbruch, Cytometry **11**, 231 (1990).
[6] A. Grützkau and A. Radbruch, Cytometry Part A **77**, 643 (2010).
[7] D. Pappas, Front Matter: Wiley Online Library (2010).
[8] S. Bhakdi, A. Ottinger, S. Somsri, P. Sratongno, P. Pannadaporn, P. Chimma, P. Malasit, K. Pattanapanyasat, and H. P. N. Neumann, Malaria J. **9**, 38 (2010).
[9] T. Baier, S. Mohanty, K. Drese, F. Rampf, J. Kim, F. Schönfeld, Microfluid Nanofluid **7**, 205 (2009).
[10] R. Gerber and P. Lawson, IEEE Trans. Magn. **25**, 806 (1989).
[11] S. Y. Wang, K. L. Mak, L. Y. Chen, M. P. Chou, and C. K. Ho, Immunology **77**, 298 (1992).
[12] W. Trager and J. B. Jensen, Science **193**, 673 (1976).
[13] C. Lambros and J. Vanderberg, J. Parasitol. **65**, 418 (1979).
[14] M. R. Potter and M. Moore, Clin. Exp. Immunol. **21**, 456 (1975).
[15] A. Scholzen, D. Mittag, S. J. Rogerson, B. M. Cooke, and M. Plebanski, PLoS Pathog. **5**, 14 (2009).
[16] S. Yilmaz, F. Unal, and D. Yuzbasioglu, Cytotech. **30**, 30 (2009).
[17] L. Ginaldi, E. Matutes, N. Farahat, M. De Martinis, R. Morilla, and D. Morilla, Br. J. Haematol. **93**, 921 (1996).
[18] H. W. Ziegler-Heitbrock, M. Strobel, D. Kieper, G. Fingerle, T. Schlunck, I. Petersmann, J. Ellwart, M. Blumenstein, and J. G. Haas, Blood. **79**, 503 (1992).
[19] B. Passlick, D. Flieger, and H. W. Ziegler-Heitbrock, Blood **74**, 2527 (1989).
[20] W. Leung and C. Civin, Clinical bone marrow and blood stem cell transplantation Cambridge University Press, Cambridge (2000).
[21] P. Lang, M. Schumm, G. Taylor, T. Klingebiel, S. Neu, A. Geiselhart, S. Kuci, D. Niethammer, and R. Handgretinger, Bone Marrow Trans. **24**, 583 (1999).
[22] T. Lea, E. Smeland, S. Funderud, F. Vartdal, C. Davies, K. Beiske, and J. Ugelstad, Scand. J. Immunol. **23**, 09 (1986).
[23] A. Winkelstein, P. L. Simon, P. A. Myers, and L. D. Weaver, Exp. Hematol. **14**, 1023 (1986).
[24] E. Bettiol, D. L. Van de Hoef, D. Carapau, and A. Rodriguez, Parasite Immunol. **32**, 389 (2010).
[25] P. M. Henson, J. Exp. Med. **134**, 114 (1971).
[26] R. Takemura, P. E. Stenberg, D. F. Bainton, and Z. Werb, J. Cell Biol. **102**, 55 (1986).